

An electromagnetic black hole made of metamaterials

Qiang Cheng, Tie Jun Cui*, Wei Xiang Jiang and Ben Geng Cai

State Key Laboratory of Millimeter Waves, Department of Radio Engineering

Southeast University, Nanjing 210096, China.

Traditionally, a black hole is a region of space with huge gravitational field, which absorbs everything hitting it. In history, the black hole was first discussed by Laplace under the Newton mechanics, whose event horizon radius is the same as the Schwarzschild's solution of the Einstein's vacuum field equations. If all those objects having such an event horizon radius but different gravitational fields are called as black holes, then one can simulate certain properties of the black holes using electromagnetic fields and metamaterials due to the similar propagation behaviours of electromagnetic waves in curved space and in inhomogeneous metamaterials. In a recent theoretical work by Narimanov and Kildishev, an optical black hole has been proposed based on metamaterials, in which the theoretical analysis and numerical simulations showed that all electromagnetic waves hitting it are trapped and absorbed. Here we report the first experimental demonstration of such an electromagnetic black hole in the microwave frequencies. The proposed black hole is composed of non-resonant and resonant metamaterial structures, which can trap and absorb electromagnetic waves coming from all directions spirally inwards without any reflections due to the local control of electromagnetic fields and the event horizon corresponding to the device boundary. It is shown that the absorption rate can reach 99% in the microwave frequencies. We expect that the electromagnetic black hole could be used as the thermal emitting source and to harvest the solar light.

*tjcui@seu.edu.cn

The concept of black hole was first introduced by Laplace under the Newton mechanics but has been widely used in the general relativity, in which a Schwarzschild black hole possesses an event horizon radius [1]. Everything hitting it including the light cannot escape from the region because the gravity potential is very powerful, and incident lights which are tangential to this circular horizon from outside would form a circle. Similarly, any object whose possible potential is so powerful that it forms an event horizon could be called as a black hole, just like a recent theoretical work reported in Ref. [3]. Actually, the absorption properties of such a black hole are similar to those of so called **black body** in thermodynamics [4]. All these black holes have a one-way surface, which absorbs all lights/particles into the horizon surface without any reflections, and hence nothing comes out from the black holes.

There are two ways to mimic the phenomena of black holes based on electromagnetic waves and metamaterials [2]. For the black hole in general relativity, the presence of matter-energy densities results in the motion of matter propagating in a curved spacetime [1]. Such a behaviour is very similar to the light or electromagnetic-wave propagation in a curved space or in an inhomogeneous metamaterial. Hence one could use the electromagnetic waves and metamaterials to mimic the celestial mechanics by comparing the refractive index to the metric of gravity [5]. Another way is to consider an analogy between the mechanics and optics [3], which is revealed by the least-action principle for the motion of particle in mechanics and the Fermat principle for the light propagation in optics [21]. This analogy generates an optical black hole [3], or an electromagnetic black hole, whose event horizon radius is just corresponding to the boundary of the device. Although the electromagnetic black is not the Schwarzschild's, it does have as good absorption behaviors as the black body, which can absorb the light waves in all directions and in a broad frequency band with high efficiency [3]. In either ways, however, the optical/photonic black holes based on metamaterials were only considered in theory and numerical simulations [3, 5], and experimental verifications have not been reported.

During the past ten years, metamaterial has been a hot research topic in the scientific community. The advances of artificial metamaterials in theories and experiments have offered scientists potent ways to tailor the properties of electromagnetic waves in the curvilinear space. Metamaterials have manifested a lot of exciting effects and devices, such as the negative refraction, electromagnetic invisibility cloaks, super-resolution imaging, electromagnetic concentrators, and light trapping [6]-[20], in which the required constitutive parameters could be fulfilled by periodic/non-periodic arrays of electric or magnetic resonant/non-resonant particles. The current technologies for designing and fabricating metamaterials have enabled people to

realize such functional devices with unusual electromagnetic properties.

In this work, we realize the electromagnetic black hole in the microwave frequencies based on the theoretical prediction to the optical black hole using non-magnetic metamaterials [3]. We have designed and fabricated the electromagnetic black hole using non-resonant and resonant metamaterial structures, and measured the internal electric fields using a planar-waveguide near-field scanning apparatus. Experimental results have good agreements to the full-wave numerical simulations, which show obvious phenomena of microwave bending and trapping spirally into the black hole and not coming back. The electromagnetic black hole can absorb electromagnetic waves coming from all directions efficiently with an absorption rate of 99%, which could find wide applications in the thermal emitting and the solar-light harvesting.

In the analytical mechanics, the motion of matter attracted by the gravitational field could be described by the Hamilton equations:

$$\frac{d}{dt}p(t) = -\frac{\partial\mathcal{H}}{\partial q}, \quad \frac{d}{dt}q(t) = \frac{\partial\mathcal{H}}{\partial p}, \quad (1)$$

in which p is the generalized momentum, q is the generalized coordinate, and \mathcal{H} is the Hamiltonian. The Hamiltonian represents energy of the system, which is the sum of kinetic and potential energy, denoted by T and V , respectively, as $\mathcal{H} = T + V$, $T = p^2/(2m)$, $V = V(q)$, in which m is the mass of matter.

In the geometrical optics, the Fermat principle determines the propagation of light. Considering that the eikonal function $S_t(r, \theta)$ in a two-dimensional (2D) cylindrical coordinate is expanded in series $S_t(r, \theta) = S(r, \theta) - \omega t$ as an Hamilton-Jacobi equation, we could get the Hamiltonian in optics as [21]

$$\mathcal{H} = \frac{\omega^2}{2\mu_0} = \frac{p_r^2}{2\epsilon(r)} + \frac{p_\theta^2}{2r^2\epsilon(r)}, \quad (2)$$

in which $p_r = \partial S/\partial r$ and $p_\theta = \partial S/\partial \theta$ are the radial and angular momentum in the cylindrical coordinate, ω is the radian frequency, μ_0 is the magnetic permeability in free space, and $\epsilon(r)$ is the electric permittivity in the isotropic non-magnetic medium. Since the frequency is invariant in a time-harmonic system, the above equation reveals an energy conservation in mechanics. From the Hamilton equation, the trajectory of geometrical optics looks like a unit particle in a central potential which is given by [3]: $V_{\text{eff}}(r) = \omega^2 c^2 [\epsilon_b - \epsilon(r)]/2$, in which ϵ_b is the background permittivity, and c is the light speed. When the inhomogeneous electric permittivity is chosen as

$$\epsilon(r) = \begin{cases} \epsilon_b, & r > R \\ \epsilon_s(r) = \epsilon_b(R/r)^2, & R_c \leq r \leq R \\ \epsilon_c + i\gamma, & r < R_c \end{cases}, \quad (3)$$

the Hamilton equation represents a Kepler problem. The above permittivity distribution describes a layered dielectric cylinder, which includes a lossy circular inner core and a lossless circular shell with radially-varied permittivity, as shown in Fig. 1(a). Here, R_c and R stand for the radii of inner core and outer shell of the cylinder, while ϵ_b and ϵ_c represent the dielectric constants of the background medium and the lossy material inside the core. The radius of core is closely related to the ratio of two dielectric constants: $R_c = R\sqrt{\epsilon_b/\epsilon_c}$. Under the ray approximation, it has been proved that the light hitting the cylinder will bend spirally in the shell region, and be trapped and absorbed by the lossy core, as illustrated in Fig. 1(a). It is also shown that the scattering cross section per unit length of the cylinder is nearly zero, which is independent of the polarization state of incident waves [3]. Hence the dielectric cylinder behaves like a 2D **black hole** and the boundary represents the event horizon, which could absorb all lights hitting it from every direction.

When the operating frequency falls into the microwave band, the ray approximation produces a certain error, which results in small scattering cross sections from the black hole. Hence we expect that the electromagnetic black hole will absorb most electromagnetic waves hitting it from every direction with tiny scattering. Next we will validate the electromagnetic black hole through numerical simulations and experiments. From Eq. (3), the permittivity distribution of the black hole's outer shell ($R_c < r < R$) varies gradually from the inner core to the background medium. Hence the outer shell can be realized by gradient refraction index metamaterials, which have been used in the design of some new concept devices such as the invisibility cloak [10] and ground cloaks [12, 13].

A number of non-resonant metallic structures could be utilized as the basic element of gradient refraction index metamaterials, such as the circular ring, I-shaped structure, and Jerusalem cross. The dimensions of unit geometries could be adjusted to meet the demand of refraction indices at specific positions, to achieve the gradient distribution. In non-resonant metamaterials, the resonant frequencies of unit geometries are much higher than the operating frequency, and the dispersion curves for effective permittivity and permeability change slowly in a broad band. Considering the anisotropy of most metamaterial unit, the electromagnetic constitutive parameters for the black hole are adjusted for the transverse-electric (TE) polarization in the cylindrical coordinate as $\epsilon_z = \epsilon(r)$, $\mu_\phi = 1$, and $\mu_r = 1$. In our design, we choose the non-resonant I-shaped structure [12] as the basic unit for the outer shell of the electromagnetic black hole, and the electric-field-coupled (ELC) resonator [19] as the basic unit for the inner core, which has large permittivity and large loss tangent simultaneously near the resonant frequency.

The photograph of the fabricated electromagnetic black hole is shown in Fig. 1(b), in which the I-shaped

unit cell and ELC resonator are illustrated in Figs. 2(a) and 2(b), respectively. The black hole is placed in the air, hence the permittivity of background medium is simply $\epsilon_b = 1$. In order to better demonstrate the absorption effect, a relatively high microwave frequency ($f = 18$ GHz) is selected in simulations and experiments. The sizes of both I-shaped unit cell and ELC resonator are set as 1.8 mm, nearly 1/10 of the free-space wavelength. The whole black hole is composed of 60 concentric layers, and each layer is a thin printed circuit board (F4B, $\epsilon = 2.65 + i0.001$) etched with a number of sub-wavelength unit structures. From Eq. (3), the permittivity changes radially in the shell of black hole, and hence the unit cells are identical in each layer but have different sizes in adjacent layers. Since the permittivity is a constant in the lossy core, the ELC resonators are identical in the whole region.

Figure 2 demonstrates the effective medium parameters of the I-shaped and ELC units for the designed black hole. The full-wave numerical tool (Microwave Studio, CST2006b) has been used to simulate the electromagnetic properties. Following the standard retrieval procedure [22], the effective permittivity and permeability are obtained from the scattering parameters with the change of geometry dimensions. To determine the relation between geometry and medium parameters, an interpolation algorithm has been developed to generate the final layout according to the permittivity distribution required by the black hole. From Fig. 2(a), by changing the height of I-shaped unit, the real part of permittivity $\text{Re}(\epsilon_z)$ ranges from 1.27 to 12.64 at 18 GHz, while the permeability components, $\text{Re}(\mu_r)$ and $\text{Re}(\mu_\phi)$, are always close to unity. The imaginary parts of permittivity and permeability for the I-shaped unit, not shown here, are small enough to be neglected in the design of black hole. From Fig. 2(b), the operating frequency is close to the resonant frequency of the ELC structure, which results in a very lossy permittivity $\epsilon_z = 9.20 + i2.65$ and lossy permeability components $\mu_r = 0.68 - i0.01$ and $\mu_\phi = 0.84 - i0.14$ at 18 GHz.

In our design, the space between adjacent layers is 1.8 mm, hence the radii of the black hole and the lossy core are determined immediately as $R = 108$ mm and $R_c = 36$ mm. There are totally 40 layers of I-shaped structures and 20 layers of ELC structures. In order to fix the 60 layers with different radii together, a 0.8-mm-thick styrofoam board has been used with 60 concentric circular slots carved by the LPKF milling machine (LPKF s100). Each layer has three unit cells in the vertical direction, and hence the height of black hole is 5.4 mm. To investigate the interactions between the fabricated black hole and incident TE-polarized electromagnetic waves, a parallel-plate waveguide near-field scanning system is used to map the field distributions near the black hole at 18 GHz. A similar apparatus has been discussed in Ref. [23]. The separation between two plates is set as 6.5 mm, which is larger than the height of black hole to

avoid the unnecessary dragging during measurements. The cutoff frequency of the waveguide system for the dominant TEM mode is 23 GHz. The bottom plate is mounted on a step motor which can translate in two dimensions. A monopole probe is fixed inside the waveguide as the feeding source, and a corner reflector is placed on the back of source to produce the desired narrow beam. Four detection probes are placed on the top plate to measure the field distributions on a plane above the black hole under test, and each probe can scan a region of 200 mm by 200 mm independently. Hence the total scanning region is 400 mm by 400 mm with a step resolution of 0.5 mm. All probes are connected to a microwave switch which controls the measurement sequence after each movement of the step motors below the bottom plate. The two ports of a vector network analyzer (Agilent PNA-L N5230C) are connected to the feeding probe and the microwave switch respectively via cables. Then the measurement data are sent to the controlling computer for post processing.

To demonstrate the performance of black hole in the microwave frequency, we first consider the case of Gaussian-beam incidence. Figures 3(a) and (b) illustrate the distributions of simulated electric fields $|E_z|$ at 18 GHz when a Gaussian beam is incident on the black hole on-center and off-center, respectively. We note that all on-center rays are directly attracted by the black hole without reflections, and nearly all off-center rays bend in the shell region spirally and are trapped by the core. To evaluate the absorption of Gaussian beam by the electromagnetic black hole, we define an absorbing rate from the Poynting theorem as

$$\eta = P_{\text{absorb}}/P_{\text{in}}, \quad P_{\text{absorb}} = -\frac{1}{2}\text{Re}\left(\oint_s \vec{E} \times \vec{H}^* \cdot d\vec{S}\right), \quad (4)$$

in which P_{absorb} is the net power entering the black-hole surface, and P_{in} is the incident power. Under the on-center and off-center incidences shown in Figs. 3(a) and 3(b), the absorbing rates are calculated as 99.94% and 98.72%, respectively. Nearly all incident powers are absorbed by the microwave black hole.

In the microwave frequency, however, it is difficult to generate the Gaussian beam. Hence we use monopole probe with corner reflector to produce the narrow beam in our experiments, as demonstrated in Figs. 3(c)-(f). Comparing with the Gaussian beam, the produced beam is divergent while propagating. Similar to Figs. 3(a) and 3(b), we measure two cases when the electromagnetic waves are incident vertically and obliquely to the black hole. As a comparison, the full-wave numerical simulations are also given to illustrate the absorption effect. Figures 3(c) and 3(e) illustrate the distributions of simulated and measured electric fields $|E_z|$ at 18 GHz for the vertical-incidence case, which agree to each other very well. It is clear that the incident beam becomes convergent inside the shell region and then enters the lossy core of black hole instead

of being divergent in the free-space radiation. The absorbing rate corresponding to Fig. 3(c) is 99.55%, nearly full absorption. When the beam is incident to the black hole at an oblique angle 25° , the waves are bent toward the central area and travel around the shell spirally with distinct absorption, as shown in Figs. 3(d) and 3(f). Again, the simulation and experiment results have good agreements. From Figure 3, the black hole is a good attractor and absorber to microwaves.

Comparing the experiment and simulation results with the theoretical prediction in the optical frequency [3], it is clear that the design for optical black hole still holds in the microwave region. Hence we realize the electromagnetic black hole experimentally in the microwave frequency, which could be used to collect microwaves and energies in free space. When the incident waves are not narrow beams, they can also be absorbed efficiently by the black hole. Figures 4(a) and 4(b) demonstrate the field and power distributions inside and outside the black hole under the incidence of plane waves (such as solar light). Obviously, nearly all incident waves hitting the black hole are trapped to the center and do not come out with the absorbing rate of 99.12%. Being absorbed by the black hole, the incident waves hitting it cannot go through, and the total fields are nearly zero in the front region, **making a complete shadow**. We also notice that the black hole nearly does not disturb the electromagnetic waves in other regions. When the incident waves are excited by a nearby monopole, the simulated and measured field distributions are shown in Figs. 4(c) and 4(d), respectively. Like the case of plane-wave incidence, nearly all incident waves hitting the black hole (see the black dashed lines) are absorbed, producing a shadow region. The simulated and measured results have good agreements.

In summary, we have designed, fabricated, and measured an electromagnetic black hole at the microwave frequency using non-resonant I-shaped metamaterials and resonant ELC metamaterials based on the theoretical study [3]. We have observed that nearly all incident waves and energies hitting the designed black hole are attracted and absorbed. The good consistence between theoretical and experimental results have shown the excellent ability for metamaterials as the candidate to construct the artificial black holes. Although the proposed electromagnetic black is not the Schwarzschild black hole, it does have as good absorption behaviors as the black body does in thermodynamics. Since the lossy core can transfer the electromagnetic energies into heat energies, we expect that the electromagnetic black hole could find important applications in the thermal emitting and the solar-light harvesting.

This work was supported in part by the National Science Foundation of China under Grant Nos. 60990320, 60990324, 60671015, 60496317, and 60901011, in part by the Natural Science Foundation of

Jiangsu Province under Grant No. BK2008031, and in part by the 111 Project under Grant No. 111-2-05.

References

- [1] Kox, A. J. et al. (eds). *The Collected Papers of Albert Einstein*. Vol. 6 (Princeton Univ. Press, 1997).
- [2] Pendry, J. B., Schurig, D. & Smith, D. R. Controlling electromagnetic fields. *Science* **312**, 1780-1782 (2006).
- [3] Narimanov, E. E., Kildishev, A. V. Optical black hole: Broadband omnidirectional light absorber. *Appl. Phys. Lett.* **95**, 041106 (2009).
- [4] Davies, P. C. W. Thermodynamics of Black Holes. *Rep. Prog. Phys.* **41**, 1313 (1978).
- [5] Genov, D. A., Zhang, S., Zhang, X. Mimicking celestial mechanics in metamaterials. *Nature Phys.* (2009).
- [6] Smith, D. R., Padilla, W. J., Vier, D. C., Nemat-Nasser, S. C. & Schultz, S. Composite medium with simultaneously negative permeability and permittivity. *Phys. Rev. Lett.* **84**, 4184-4187 (2000).
- [7] Smith, D. R., Pendry, J. B. & Wiltshire, M. C. K. Metamaterials and negative refractive index. *Science* **305**, 788-792 (2004).
- [8] Zhang, X. & Liu, Z. W. Superlenses to overcome the diffraction limit. *Nature Mater.* **7**, 435-441 (2008).
- [9] Soukoulis, C. M., Linden, S. & Wegener, M. Negative refractive index at optical wavelengths. *Science* **315**, 47-49 (2007).
- [10] Schurig, D. *et al.* Metamaterial electromagnetic cloak at microwave frequencies. *Science* **314**, 977-980 (2006).
- [11] Leonhardt, U. Optical conformal mapping. *Science* **312**, 1777-1780 (2006).
- [12] Liu, R., Ji, C., Mock, J. J., Chin, J. Y., Cui, T. J., Smith, D. R. Broadband ground-plane cloak. *Science* **323**, 366-369 (2009).
- [13] Valentine, J., Li, J., Zentgraf, T., Bartal, G. & Zhang, X. An optical cloak made of dielectrics. *Nature Mater.* **8**, 568-571 (2009).

- [14] Cai, W. S., Chettiar, U. K., Kildishev, A. V. & Shalaev, V. M. Optical cloaking with metamaterials. *Nature Photon.* **1**, 224-227 (2007).
- [15] Leonhardt, U. & Tyc, T. Broadband invisibility by non-euclidean cloaking. *Science* **323**, 110-112 (2009).
- [16] Greenleaf, A., Kurylev, Y., Lassas, M. & Uhlmann, G. Electromagnetic wormholes and virtual magnetic monopoles from metamaterials. *Phys. Rev. Lett.* **99**, 183901 (2007).
- [17] Ma, G. M., C. K. Ong, Tyc, T. & Leonhardt, U. An omnidirectional retroreflector based on the transmutation of dielectric singularities. *Nature Mater.* **8**, 639-642 (2009).
- [18] Jiang, W. X., Cui, T. J., Cheng, Q., Chin, J. Y., Yang, X. M., Liu, R., Smith, D. R. Design of arbitrarily shaped concentrators based on conformally optical transformation of nonuniform rational B-spline surfaces. *Appl. Phys. Lett.* **92**, 264101 (2008).
- [19] Schurig, D., Mock, J. J. & Smith, D. R. Electric-field-coupled resonators for negative permittivity metamaterials. *Appl. Phys. Lett.* **88**, 041109 (2006).
- [20] Tsakmakidis, K. L., Boardman, A. D., & Hess, A. ‘Trapped rainbow’ storage of light in metamaterials. *Nature* **450**, 397-401 (2007).
- [21] Landau, L. D., & Lifshitz, E. M. *The Classical Theory of Fields*, 4th ed. (Butterworth Heinemann, 1999).
- [22] Smith, D. R., Schultz, S. , Markos, P. & Soukoulis, C. M. Determination of effective permittivity and permeability of metamaterials from refraction and transmission coefficients. *Phys. Rev. B*, **65**, 195104 (2002).
- [23] Justice, B. J. *et al.* Spatial mapping of the internal and external electromagnetic fields of negative index metamaterials. *Opt. Express*, **14**, 8694 (2006).

List of Figure Captions

Fig. 1: (color online) (a) A model of black hole composed of a gradient-index metamaterial shell and a lossy dielectric core. (b) Photograph of the fabricated artificial black hole based on metamaterials, which is composed of 60 concentric layers, with ELC structures in the core layers and I-shaped structures in the shell layers.

Fig. 2: (color online) Effective medium parameters for unit cells of the artificial black hole. (a) The relation between the effective permittivity (real part of ϵ_z) and permeability (real parts of μ_r and μ_ϕ) and the geometry dimension m for the I-shaped unit. The inset shows the sketch of the I-shaped unit, with $w = 0.15$ mm and $q = 1.1m$. (b) The effective permittivity (real and imaginary parts of ϵ_z) and permeability (real parts of μ_r and μ_ϕ) versus to the frequency for the ELC resonator. The inset shows the sketch of the ELC unit, where $t = 1.6$ mm, $g = 0.3$ mm, $p = 0.15$ mm, and $s = 0.65$ mm.

Fig. 3: (color online) Distributions of electric fields $|E_z|$ for the designed black hole at the frequency of 18 GHz. An electric monopole is placed inside a corner reflector to produce the desired incident beam with finite width. The two circles stand for boundaries of the outer shell and the inner core. (a) The full-wave simulation result under the on-center incidence of a Gaussian beam. (b) The full-wave simulation result under the off-center incidence of a Gaussian beam. (c) The full-wave simulation result under the vertical incidence of the produced narrow beam. (d) The full-wave simulation result under the oblique incidence of the produced narrow beam. (e) The experimental result under the vertical incidence of the produced narrow beam. (f) The experimental result under the oblique incidence of the produced narrow beam.

Fig. 4: (color online) (a) Distributions of electric fields for the electromagnetic black hole at the frequency of 18 GHz when a plane wave is incident. (b) Distributions of power flows for the electromagnetic black hole at the frequency of 18 GHz when a plane wave is incident. (c) Full-wave simulation results of electric fields under the excitation of a monopole at 18 GHz. (d) Experimental results of electric fields under the excitation of the monopole at 18 GHz.

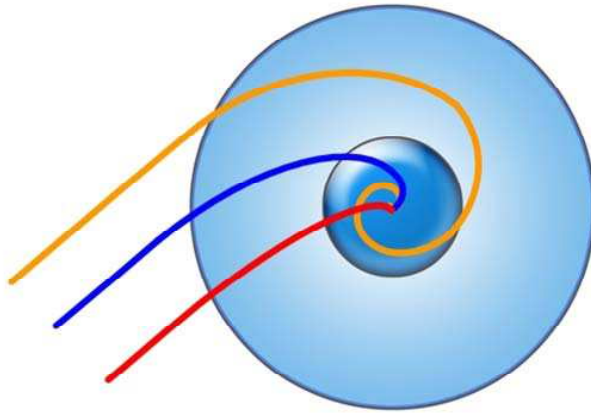
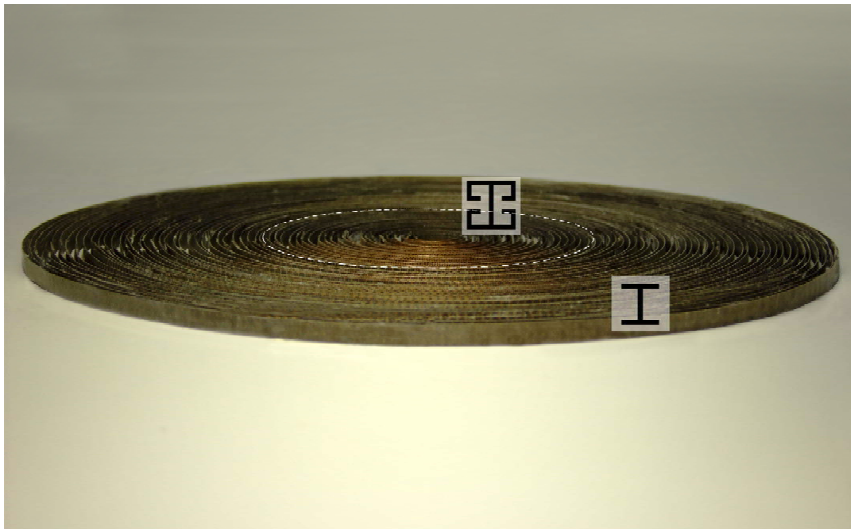
a**b**

Figure 1:

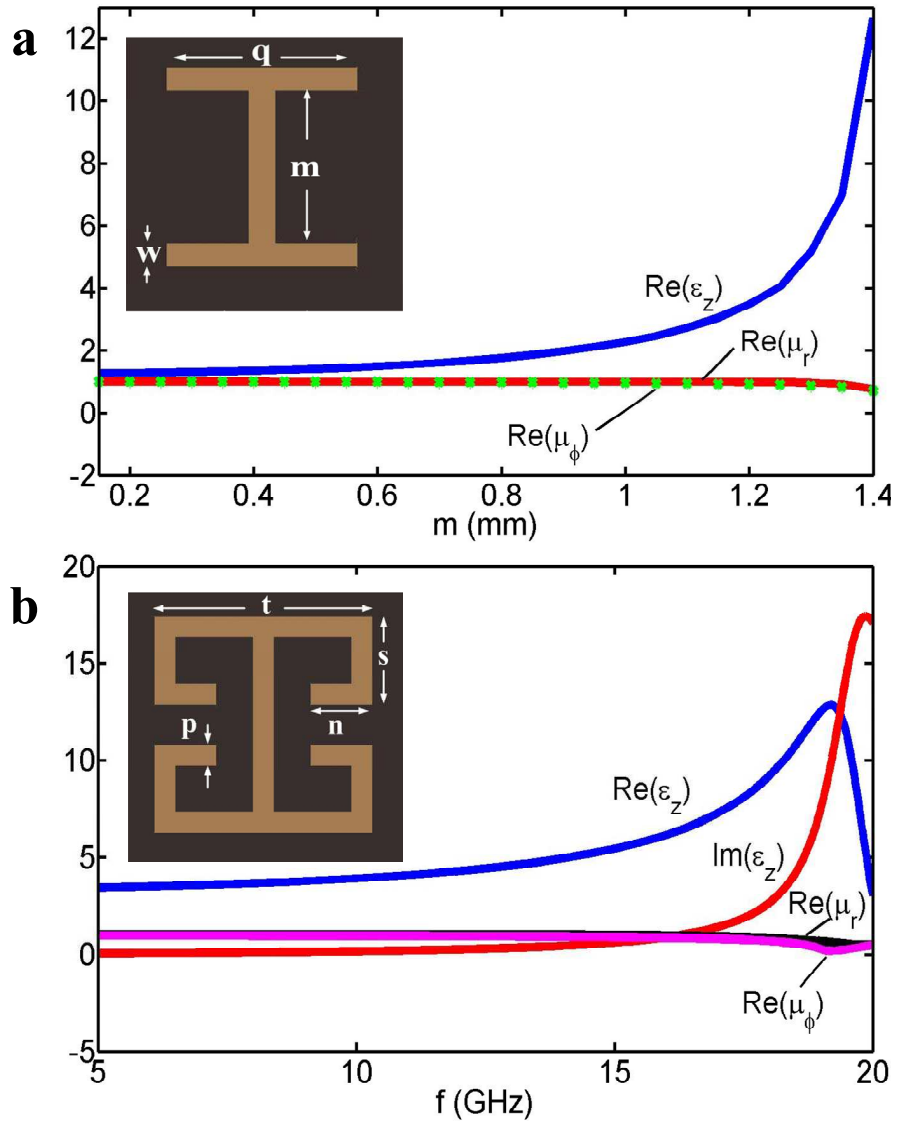


Figure 2:

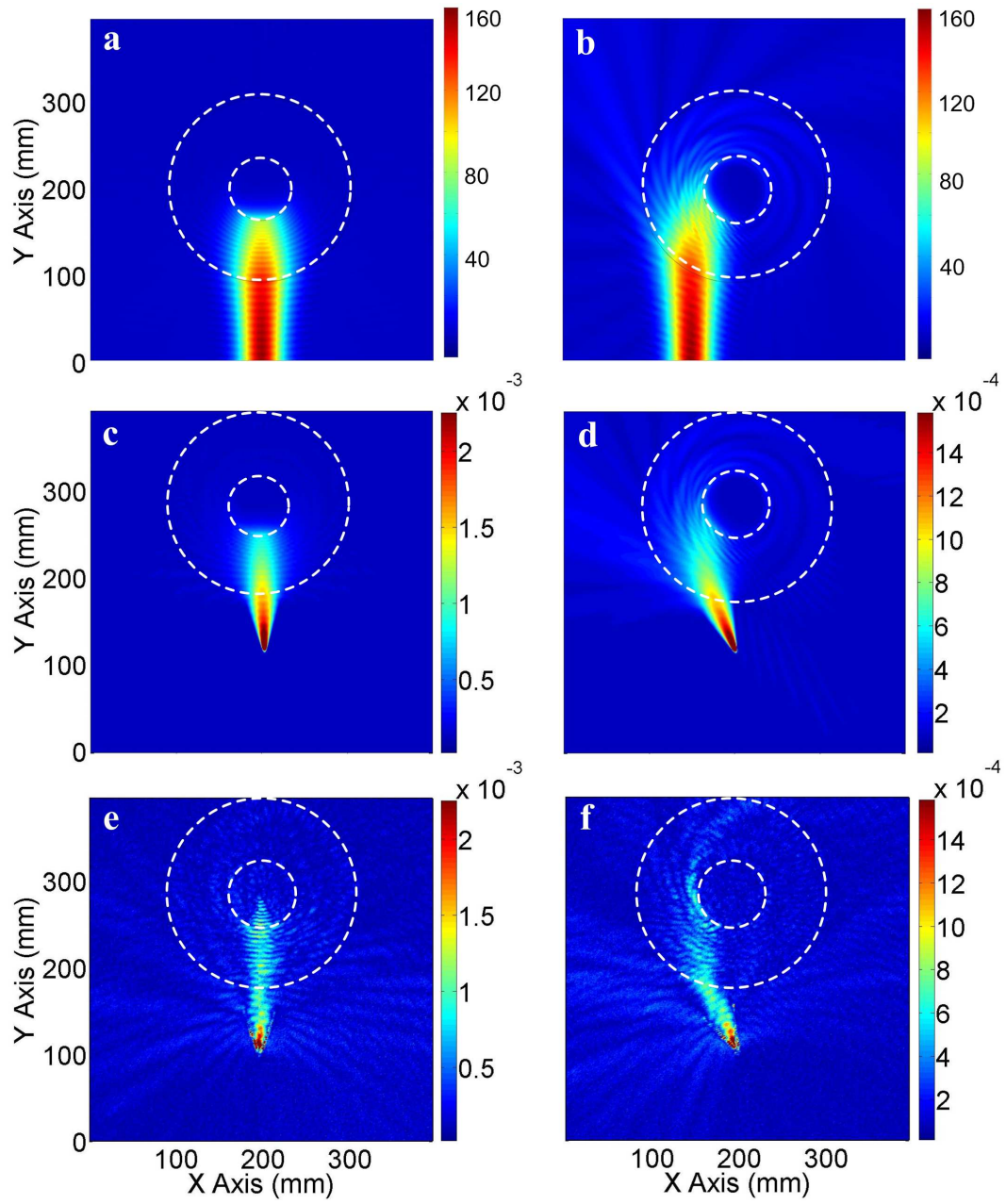


Figure 3:

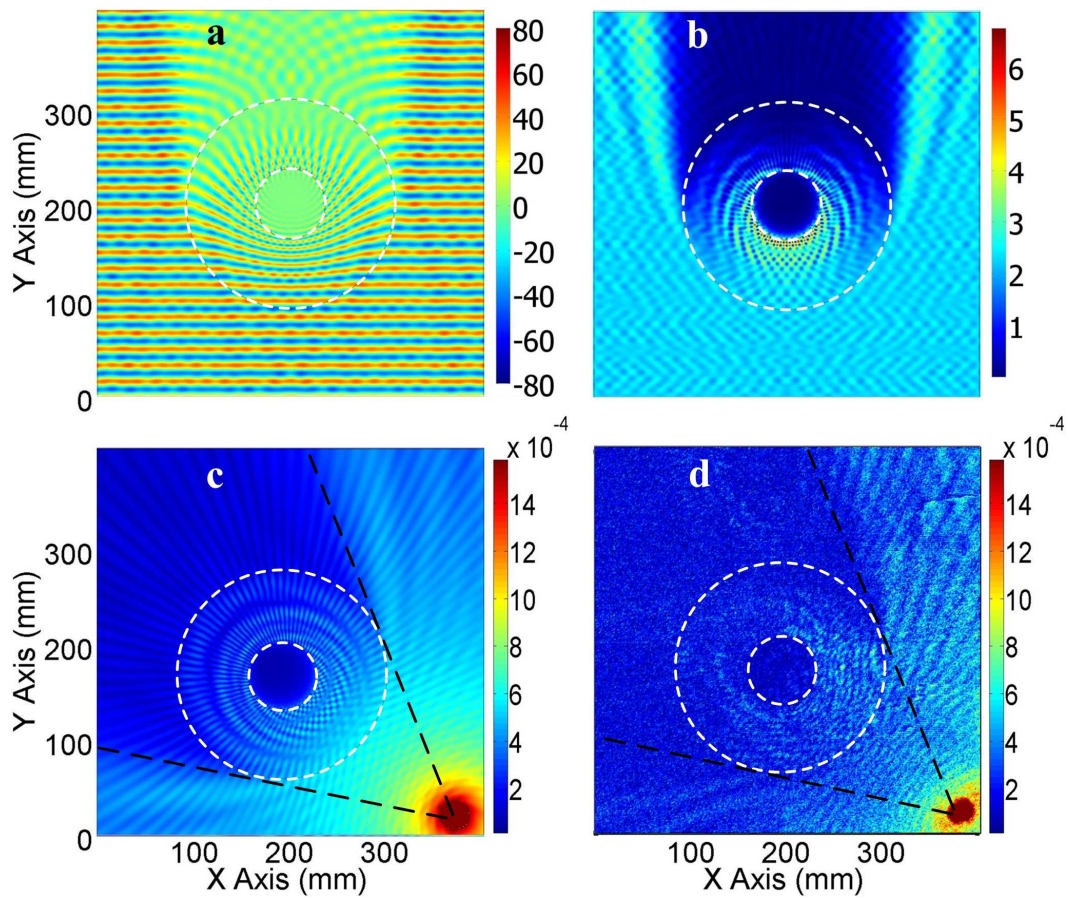


Figure 4: